

DOE/BC/14850--4

4Q/96
BC/14850-4

RESERVOIR ENGINEERING RESEARCH
INSTITUTE

Rec. 3/28/97


Fractured Petroleum Reservoirs

DE-FG22 - 93BC14850

February 20, 1997

RECEIVED

JUL 2 / 1998

OSTI

Reporting Date: 10/3/96 to 12/31/96

Principal Authors:
Dr. Abbas Firoozabadi
Dr. Mehran Pooladi-Darvish

Quarterly Report

MASTER

DISTRIBUTION OF THIS DOCUMENT IS UNLIMITED
LAU

845 Page Mill Road
Palo Alto, CA 94304

**RESERVOIR ENGINEERING RESEARCH
INSTITUTE**

**PROJECT 5: SOLUTION GAS DRIVE
IN HEAVY OIL RESERVOIRS**

**Gas and Oil Phase Mobilities in
Cold Production of Heavy Oils**

4Q.96

October 1 through December 31, 1996

Mehran Pooladi-Darvish
Abbas Firoozabadi

DISCLAIMER

This report was prepared as an account of work sponsored by an agency of the United States Government. Neither the United States Government nor any agency thereof, nor any of their employees, makes any warranty, express or implied, or assumes any legal liability or responsibility for the accuracy, completeness, or usefulness of any information, apparatus, product, or process disclosed, or represents that its use would not infringe privately owned rights. Reference herein to any specific commercial product, process, or service by trade name, trademark, manufacturer, or otherwise does not necessarily constitute or imply its endorsement, recommendation, or favoring by the United States Government or any agency thereof. The views and opinions of authors expressed herein do not necessarily state or reflect those of the United States Government or any agency thereof.

DISCLAIMER

**Portions of this document may be illegible
electronic image products. Images are
produced from the best available original
document.**

Oil and Gas Phase Mobilities in Cold Production of Heavy Oils

Summary

In this report, we present the results of our first experiment on a heavy crude of about 35,000 cp. A new visual coreholder was designed and built to accommodate the use of unconsolidated sand. From this work, several clear conclusions can be drawn: 1) oil viscosity does not decrease with the evolution of gas, 2) the critical gas saturation is in the range of 4-5%, and 3) the endpoint oil relative permeability is around 0.6. However, the most important parameter, gas phase mobility, is still unresolved. Gas flows intermittently, and therefore the length effect becomes important. Under the conditions that we run the experiment, recovery is minimal, about 7.5%. This recovery is still much higher than the recovery of the C_1/C_{10} model system which was 3%. After a duplicate test, we plan to conduct the experiment in the horizontal core. The horizontal core is expected to provide a higher recovery.

Introduction

Production from some of the heavy oil reservoirs in Canada and Venezuela has given unexpectedly high oil rates and recoveries under solution gas drive. In an early paper, Smith [1988] reported this behavior in the heavy oil reservoirs of the Lloydminster area, Canada. Analysis of the field data showed production rates much in excess of that predicted by the Darcy law [Smith 1988]. Similarly, Loughhead and Saltuklaroglu [1992] and Metwally and Solanki [1995] reported solution gas drive oil recoveries as high as 14% and flow rates of one order of magnitude larger than the predictions of the Darcy radial flow. These and other authors reported co-production of large volumes of sand and the delayed liberation of gas from the wellhead crude samples in open vessels. More recently, similar behavior was reported in some of the heavy oil reservoirs in Venezuela. Mirabal et al. [1996] presented examples of high flow rates under solution gas drive from one of the heavy oil reservoirs of the Orinoco Belt. In addition to the unexpectedly high production rates, the reservoir pressure was nearly maintained in the 12 years of production history.

In order to explain the above behavior, a number of mechanisms have been suggested which can be divided into two main categories; geomechanical effects, such as sand dilation and flow and the development of wormholes comprise the first category. The second category, which is the subject of the current research, suggests that the special properties of the flowing fluids, the gas and the heavy oil, are the main reasons for high production performance.

The effect of other pressure maintenance mechanisms such as an active aquifer and the reservoir compaction have been found small in these reservoirs [Smith 1988, Loughhead and Saltuklaroglu 1992, Mirabal 1996]. Due to production, the pore pressure drops below the bubble point pressure to a critical supersaturation pressure, and then gas evolves in the reservoir. If the evolved gas is retained in the reservoir, two-phase compressibility will be high [Smith 1988, Loughhead and Saltuklaroglu 1992], and the reservoir pressure declines

slowly [Mirabal et al. 1996]. A number of mechanisms have been proposed to explain the low gas mobility. Kraus et al. [1993] proposed that below bubble point, the evolved gas is retained in the porous media until the pressure reduces to a lower pressure, called pseudo bubble point pressure. Below the pseudo bubble point pressure, some of the evolved gas forms a continuous gas phase. Claridge and Prats [1995] in a similar analysis suggested that all of the evolved gas below the bubble point pressure is kept in the form of small bubbles in the porous media and does not form a continuous free gas phase. Formation of a "semi-rigid coating" of asphaltene components at the gas-oil interface was proposed to explain the lack of coalescence of the gas bubbles.

In contrast to the above modifications in the pressure-dependent properties, Sheng et al. [1995] proposed a model for time-dependent physical properties of the fluids. These authors used the proposed model to match the volume behavior of a live oil sample when its pressure was abruptly reduced from 700 psi to 350 psi. Smith [1988] and other authors have reported that the volume of the produced crude in the tanks at the well site reduces considerably with time. Huetra et al. [1996] discussed time-dependent behavior when they increased the volume of a live oil sample in a cylinder in discrete steps. Following each expansion, it took twenty four hours before pressure increase became negligible. The authors made bubble point measurements with no agitation. The data show non-equilibrium effects; the total volume at all pressures below the bubble point was lower than the equilibrium volume. This is a clear indication of supersaturation. The time-dependent behavior under field conditions with time-scales much larger than those pertaining to laboratory experiments has not been fully addressed yet. It is likely that time-dependent properties, with time-scales of the order of 40 minutes [Sheng et al. 1995] to 24 hours [Huerta et al. 1996] are not the primary reasons for the performance of heavy oil reservoirs under solution gas drive.

Smith [1988] suggested that the evolved gas below the bubble point pressure forms very tiny bubbles, and the bubbles are carried with the flowing oil phase; they do not coalesce to form a continuous gas phase. Maini et. al. [1993] performed steady state solution gas drive experiments in a 1-D sand pack; the inlet pressure was kept at the bubble point pressure and the outlet pressure was dropped in steps of 48 psi. The authors observed production of gas-oil mixture in the form of foam at the outlet and suggested that a non-aqueous foam is generated inside the porous media, in which the oleic phase is the continuous phase. The foamy behavior was used to explain the existence of high gas saturation in their experiments. Firoozabadi and Anderson [1994] performed solution gas drive experiments in a 8" long Berea sandstone housed in a transparent core-holder. Presence of an open window at one end of the core permitted visualization of the producing fluid at the flowing pressure. The authors observed appearance and growth of the gas bubbles on the core surface. Discrete flow of gas streams into the window was observed. Based on this observation, they rejected the notion of simultaneous flow of tiny gas bubbles with the oil stream. The gas saturation at which gas flow occurred, i.e., critical gas saturation was 2.5-3% for two tests on an 11-API crude. It was concluded that the critical gas saturation for heavy oil systems may be in the range of light crudes. Upon further expansion, more oil was recovered, until gas saturations as high as 10% were

developed in the core. Based on this observation, the authors suggested that gas mobility may remain low in a heavy oil system. Huerta et al. [1996] used a heavy oil saturated sand-pack and performed solution gas drive experiments at a constant production rate. The authors reported a "mobile gas saturation" of 10%, apparently inferred from the plot of GOR vs. pressure. In a recent study, Bora et al. [1997] reported solution gas drive experiments in a micro-model. They did not observe simultaneous flow of a large number of micro-bubbles with the oil stream. Depending on the rate of depletion, one to several nuclei were formed, grew and flowed toward the production side. Nucleation occurred at the pore walls and in the trapped layer of water in the water-wet media. Other nucleation sites were location of trapped impurities and boundaries between water-wet and oil-wet media [Bora et al. 1997].

The emphasis of majority of the above studies is on the gas phase; its behavior and interaction with the heavy oil is used to explain the high production performance of heavy oil reservoirs under solution gas drive. Claridge and Prats [1995] proposed that asphaltene components of the heavy oil separate from the oil and concentrate at the gas-oil interface; the asphaltenes separation from oil leads to a much lower oil viscosity and enhanced oil mobility. Shen and Batycky [1996] suggested that lubrication effects due to the presence of the nucleated gas at the pore walls enhances oil mobility. They proposed an equation for the effective viscosity of the foamy oil incorporating the lubrication effect, which was then used by the authors to match the experimental data of Maini et al. [1993]. In order to address the issue of the apparent viscosity of the fluid below bubble point pressure, Huerta et al. [1996] used a 6 m long slim tube for solution gas drive under constant production rate. These authors did not observe a significant change in pressure drop until the saturation approached the critical gas saturation. Close to the critical gas saturation, pressure drop increased gradually to as much as 40-70%; no oil mobility improvement was evidenced in their experiments.

The focus of this project is the understanding and modeling of gas and oil phase mobilities. In this work, we measure the critical gas saturation in an unconsolidated sand pack saturated with a light model oil and a heavy crude. We define the critical gas saturation as the minimum gas saturation at which gas flow can be sustained, which differs from the definition by Maini et al. [1993] based on continuity of the gas phase. We also study the behavior of gas evolution in a heavy oil-saturated porous medium, and compare it with the light model oil. One goal is to use the experimental results to examine the mechanisms suggested in the literature.

Experimental

Figure 1 shows the schematic diagram of the experimental setup. The main component is the visual core-holder. An ISCO pump is used for saturating the porous medium and producing the oil during the depletion. Other components are; a high pressure cylinder used for preparation of the live oil, pressure and temperature sensors, and a video camera for detecting the onset of gas flow. All of the above components are housed in a temperature-controlled air bath. Acquisition of the pressure data, and control of the

temperature of the bath is performed with a PC, and the video image is stored using a recorder.

The body of the core-holder is made of an acrylic tube with a wall thickness of 12 mm. The top components of the core-holder were especially designed to provide the seal while exerting pressure on the sand pack. This would ensure that the seal displaces the space from the compaction of the sand during different stages of the experiment. The top components are two stainless steel disks with a 12 mm thick rubber sandwiched between them (see the exert in Figure 1). The lower disk which sits on the sand has a stainless steel screen to avoid sand flow, and a set of groves to facilitate production of the fluids. A 6-mm OD stainless steel tubing, welded to the lower disk, passes through the rubber and the upper disks and ends in a window made inside an acrylic rod. The fluid produced from the sand pack enters the window and flows out through a side tubing drilled through the acrylic rod. The window is graduated to measure the gas volume. Connections between the core-holder, the pressure transducers and the pump are made of 3 mm OD stainless steel tubings. The total dead volume at the top of the ISCO pump, in the tubings, and transducers is about 16 cm³.

Rock and Fluid Data

Clean Ottawa sand with a grain size of 212 - 355 μ m comprised the porous medium. The top of the sand pack was covered with 6 mm layer of coarse sand grains (600 - 800 μ m). The openings of the screen at the top of the sand were 425 μ m. This configuration was used to avoid sand flow through the screen, and to prevent gas hold-up below the stainless steel screen. The sand pack was prepared by pouring small batches of clean sand into the core-holder and pounding on it. A thin layer of the coarse sand was then added to the top of the pack and the components were assembled. By tightening the screws at the outlet cap a uni-axial pressure was exerted on the sand column. The pressure caused expansion in the rubber disk which provided the seal. Permeability and porosity of the sand pack were 16 Darcy and 36%. Other relevant data are provided in Table 1.

Methane was used as the gas phase in all of the experiments. Normal decane and a heavy crude were used for the light model oil and heavy oil runs, respectively. Table 2 gives some of the physical properties of the fluids. Small amount of water was present in the heavy crude. The GOR for the light and heavy oils were 13 and 6 vol/vol, respectively. The approximate bubble point pressure of the two fluids were 280 and 300 psig, respectively.

In order to obtain a qualitative measure of gas evolution, the live heavy oil was expanded in an atmospheric separator, and the volume of the oleic phase was recorded. Oleic phase refers to the oil with the gas bubbles inside. Figure 2 shows the liquid volume with time. Initially, the volume of the oil increased as bubbles formed on the surface. This was followed by a continuous reduction in liquid volume for more than one day. It took about five minutes to accumulate enough liquid in the separator. Figure 2 shows that the volume of the oil decreased considerably.

Test Procedure

The core-holder was assembled on a frame that could rotate 180 degrees, and vacuum was pulled on the system. The syringe pump was then filled with the dead oil, and the entire system was saturated. The system pressure was increased to 500 psig. After performing a permeability measurement, the remaining oil in the pump was removed and the pump was filled with the live oil at a pressure twice of the bubble point pressure. The dead oil in the lines and in the core were then displaced with at least 1.5 PV of live oil. This took about five hours for the light oil and about three days for the heavy oil. The lowest pressure in the system was at least 30% above the bubble point pressure. In the case of the heavy oil experiment, constant flow rate of live oil through the sand pack was used for calculating the viscosity of the live oil. The system was allowed to stabilize for at least one day before the depletion test was initiated.

The live oil was prepared in a high pressure cylinder by mixing the gas and the dead oil. For the heavy oil sample, the oil was heated and mixing was continued for many days. The GOR of the live oil was used as a measure of uniformity of the fluid in the cylinder. Whenever a new live oil sample was prepared, its bubble point pressure was measured in the syringe pump by slowly expanding the volume and recording the pressure. When critical supersaturation pressure was detected, the expansion was stopped and the maximum pressure attained was taken as an estimate of the bubble point pressure. The pressure rise in the case of the light oil and heavy oil were 65 and 120 psi, respectively. (The rate of pressure decline for the heavy oil was many times of the light oil.) The estimated bubble point pressures in our experiments are believed to be accurate to within ± 10 psi.

Depletion started by operating the pump at a constant rate of withdrawal. The pressure decreased to below the bubble point pressure; at the critical supersaturation pressure gas evolved in the porous media. The onset of gas nucleation was evidenced from the pressure behavior as will be discussed later. Expansion of the gas bubbles were observed on the surface of the sand pack. Pressure data, total production and gas production data were recorded. The gas production was read from the graduations of the window at the top of the core-holder. After the window was full, the additional volume of the gas, which had entered the pump, was estimated by measuring the two-phase compressibility in the pump. It took only a few minutes to isolate the core from the pump and to measure the two-phase compressibility and to return the system to the conditions prior to isolation.

After completion of one experiment, the extra gas in the pump was released, the core-holder was rotated 180 degrees and oil from the pump was injected into the core. The gas in the window, now at the bottom, was displaced into the core and was dissolved in the oil. When the single phase fluid was established in the core, the pump was filled with fresh live oil and the fluid in the core was displaced again with at least 1.5 PV of the live oil.

Results

Two light model oil runs were performed using a C₁/C₁₀ mixture. These tests were intended to be duplications, and the results would be compared with the behavior of a heavy oil run which will be explained later.

Light Oil Experiments

Figures 3 and 4 show pressure vs. expansion for Run 1 and Run 2. The pressure is from the readings of the bottom transducer. In Run 2 expansion was started from an initial pressure of 302 psig, about 20 psi above the bubble point pressure. The rate of expansion was 0.018 cm³/hr. The rate of pressure drop in the single phase liquid was about 48 psi/day. Due to the low viscosity of the oil, the differential pressure transducer did not detect a pressure difference. The resolution of the differential pressure transducer was about 0.02 psi and that of the main transducers about 0.5 psi. Upon expansion, the liquid pressure decreased to a value of 272 psig at 0.28 cm³ expansion, when the pressure trend reversed. The pressure increased to a maximum of 280 psig in about 10 hours. At this time, the pressure started to decrease at a much lower rate compared to the single phase region. The critical supersaturation pressure and the maximum pressure after critical supersaturation of Run 1 were 2-3 psi lower than the corresponding values for Run 2. The critical supersaturation for the corresponding values for Run 1 occurred 0.02 cm³ later than Run 2.

During the course of the experiment, the rate of withdrawal was increased at two different times. The data with other relevant information are given in Table 3. Every time the rate of expansion increased, the P-V curve became steeper, indicating an increase of 1 to 2 psi in supersaturation. Despite this increase in supersaturation, the steepness of the P-V curve has a reducing trend from the beginning to the end. Calculations using the Peng-Robinson EOS show that the equilibrium curve for C₁/C₁₀ mixture has a constant slope. Reduction of steepness as observed in Figure 4 suggests that the general trend is a reduction in supersaturation. Figure 4 shows that there is about 5 psi pressure difference between the two runs. The difference does not provide good reproducibility.

In these two runs, the temperature of the core was controlled within +- 0.1 F, however, occasional failures in the operation of the control system caused temperature variation as high as 1 F (see Table 3.)

Gas evolution in the pack and recovery performance: In Run 2 at a gas saturation of 0.1%, two small bubbles were observed in the lower half of the core. Each bubble covered a few grains. The number and the size of the bubbles increased during the 10 days of depletion. The additional bubbles may have been created due to pressure disturbances that were caused by changing the rate of withdrawal, or they could be the bubbles that were created inside the sand pack. Later, some of the bubbles grew in height to about 3 cm.

At a gas saturation of 1.5%, fifty small bubbles flowed within 10 minutes into the window and occupied a volume of about 0.5 cm³. Figure 5 shows the bubbles formed on the surface of the core-holder. This picture is taken after the gas flow, and the accumulated

gas can be seen in the top window. Two sets of gas bubbles can be seen in the picture. Two gas bubbles at the left side of the graduated ruler are formed at about 7" from bottom of the core on the surface of the core. A similar bubble but smaller can be seen at 6.5" to the very right of the picture. Other bubbles can be seen between 3.5" to 5.5" mostly to the right of the ruler, which show a much lower contrast in color. These bubbles have been possibly formed inside the pack and have expanded toward the core surface. The local gas saturation on the surface of the core is less for these bubbles than the first group, making the color difference weak.

The saturation at which gas flow occurred is considered as the critical gas saturation. At this stage, gas flow into the window continued at a frequency of 2 to 4 times per day. Hence the critical gas saturation for Run 2 was 1.5%. The critical gas saturation of Run 1 was 1.3%. Figure 6 shows the increase of gas saturation in the core for Runs 1 and 2. With further expansion gas saturation increased to a maximum of 2.9%, when gas was the only producing fluid for three days. The maximum gas saturation for Run 1 was 2.6%. To obtain the gas volume in the core, the gas volume in the window and pump was subtracted from the total expansion beyond bubble point pressure. Errors due to the expansion of core-holder, and the effect of hydrostatic pressure are insignificant. If the changes in formation volume factor of the oil are neglected, the gas saturation in the core is equal to oil recovery.

Although not identical, the data of Runs 1 and 2 and the observed behavior are close enough to provide a basis for comparison between the light oil and heavy oil experiments.

Heavy Oil Experiments

We performed a single test for an 11-API heavy oil at an initial expansion rate of 0.041 cm³/hr. Figures 7 and 8 show the variation of pressure vs. volume expansion. In addition to the pressure, the pressure drop across the core is also shown. The differential pressure data in Figure 7 are the five-point average of the data, except the first four data. At the onset, the pressure differential increased from zero to 0.14 psi. The pressure data clearly show that the transient effects due to initiation of flow die out in a short time, and a constant differential pressure of about 0.14 psi is registered. From the pressure drop the live oil viscosity is calculated to be about 38000 cp.

Critical supersaturation pressure was detected at an expansion of 1.2 cm³ and 250 psig pressure. Then the pressure increased to 277 psig, about 20 psi less than the estimated bubble point pressure. Figure 7 clearly shows that upon evolution of the gas phase in the porous media, the differential pressure increases. This trend continues until expansion of about 3 cm³, corresponding to a gas saturation of 0.9%. By this time, the differential pressure has increased about 50%. We did not observe a liquid mobility enhancement suggested in the literature by several authors [Claridge and Prats 1995, Shen and Batycky 1996]. Beyond this point, and until the withdrawal rate was doubled, no significant change in the differential pressure was observed. The anomaly in the data at 5.1 cm³ expansion corresponds to the failure of the temperature control system, and is due to the effect of temperature change on the reading of the pressure transducer (see Table 3). The rate of

withdrawal was doubled at expansion of 5.95 cm^3 . This caused an additional 1-2 psi for a few hours. When we doubled the withdrawal rate, the pressure drop increased from 0.21 to 0.37 psi.

Attempts to observe gas bubbles on the surface of the core were unsuccessful until a few hours prior to rate increase, when 8 bubbles mostly in the upper half of the core were observed. One explanation for not seeing the bubbles at an earlier time is that the bubbles could have formed inside the porous media and not on the surface. The size and the number of bubbles increased with time. For example at an expansion of 11.7 cm^3 ($S_g=4.5\%$) 12 bubbles could be distinguished on the core surface. In addition to these, some of the gas bubbles at the top of the core had grown in length and had many branches. At about this time, two small bubbles were seen in the corner of the window at the top of the core. The differential pressure transducer shows reduced response in this interval. At expansion of 12.5 cm^3 , there was 0.5 cm^3 gas at the top of the window. This leads to a gas saturation of 5.1% in the core; the critical gas saturation for this experiment is estimated to be 4.5 - 5.1%.

Upon further expansion, the gas volume increased in the window. Figure 9 shows the variation of the gas saturation in the sand pack vs. expansion. Gas saturation increased to a maximum of 7% at expansion of 25 cm^3 . The flow of gas into the window, unlike the light model oil, could not be observed. Expansion of the gas volume in the window was gradual. The pressure fluctuations detected by the differential pressure transducer, however, may relate to gas flow in the core. Figure 10 clearly shows the periodic fluctuations in the pressure data (every 2 cm^3 corresponds to one day). In the case of the light oil, each gas release was accompanied with flow of approximately 0.5 cm^3 gas into the window. This took only a few minutes. Clearly, the expansion in this time interval is much less than the volume of the released gas. Therefore, following a gas flow, direction of oil flow could reverse to fill the pores which released the gas. The fluctuations in the pressure data in Figure 8 and the reduction of the differential pressure to negative values, can be explained by the reversal in the direction of oil flow. Note that beyond an expansion of about 26 cm^3 , gas flow occurred from the window into the pump. Hence the differential pressure data may have been affected by non-continuous two-phase flow in the tubings. If the upper limit of the differential pressure values in Figure 10 (or 8, before expansion of 26 cm^3) can be taken as representative of oil flow, then the data suggests that relative permeability to oil stayed in the neighborhood of 0.5, while gas saturation increased to about 7%.

After expansion of 33.9 cm^3 , the pump was stopped, and the core was isolated from the pump. The readings of the differential pressure transducer reduced from 0.1 psi to zero. In the next twenty hours, no increase was noticed in the readings of the main transducers. This indicates that by the end of experiment, the initial supersaturation had vanished. In other words, in the course of twenty days of the experiment, with an average two-phase rate of pressure drop of 6 psi/day, the time-dependent behavior had ceased.

Summary and Discussion

A solution gas drive experiment was performed in a 16 Darcy sand pack, using an 11- API Californian heavy crude of 56000 cp dead oil viscosity. The GOR, bubble point pressure and live oil viscosity were 6 vol/vol, 300 psig, and 38000 cp, respectively. For a pressure drop of 140 psi/day in the single liquid phase, critical gas saturation and maximum recovery were 4.5 - 5.1% and 7%, respectively. Three important observations related to this experiment are:

1. None of the liquid mobility improvement mechanisms suggested in the literature were observed.
2. The relative permeability to oil at critical gas saturation (end-point liquid relative permeability) was around 0.6.
3. At the end of 20 days of the experiment, the time-dependent phenomena were not detectable.

In addition to the heavy oil experiment, a C1/C10 mixture with GOR of 13 and a bubble point pressure of 280 psig was used for two solution gas drive experiments. With rate of pressure drop of 50 psi/day in the single phase, critical and maximum gas saturations were 1.5% and 3%, respectively. Gas bubbles grew areally, and formed gas patches on the core surface. For the heavy oil, the number of gas bubbles was more and they grew in dendric shapes. Despite the experimental differences between the two systems, the following can be mentioned. The mechanism of bubble formation in the heavy oil led to the formation of a larger number of bubbles. This could partly be due to higher supersaturation at the onset of bubble formation. Larger number of bubbles lead to a larger critical gas saturation. For the heavy oil, factors such as high viscosity and presence of surface-active polar components can reduce bubble coalescence, resulting in a larger bubble density, therefore lower gas mobility. Low gas mobility leads to higher oil recovery, especially in large samples. Further experiments are planned to study the effect of length on oil recovery. Simulation studies will be used for matching the experiments and scale-up to field conditions. Other experiments will focus on the effect of crude type, absence and presence of asphaltene, and the effect of the gravity force on oil recovery. The issue of gas mobility in the presence of heavy oil will be studied in depth.

References

Bora, R., Maini, B.B., and Chakma, A.: "Flow Visualization Studies of Solution Gas Drive Process in Heavy Oil Reservoirs Using a Glass Micromodel," paper SPE 37519 presented at the 1997 SPE Thermal Operations and Heavy Oil Symposium, Bakersfield, CA, Feb. 10-12.

Claridge, E.L. and Prats, M.: "A Proposed Model and Mechanism for Anomalous Foamy Heavy Oil Behavior," paper SPE 29243 presented at the 1995 SPE International Heavy Oil Symposium, Calgary, AB, June 19-21.

Firoozabadi, A. and Anderson, A.: "Visualization and Measurement of Gas Evolution and Flow of Heavy and Light Oil in Porous Media," paper SPE 28930 presented at the 1994 SPE Annual Technical Conference and Exhibition, New Orleans, LA.

Huerta, M., Tico, A., Jimenez, I, de Mirabal, M., and Rojas, G.: "Understanding Foamy Oil Mechanisms for Heavy Oil Reservoirs During Primary Production," paper SPE 36749 presented at the 1996 SPE Annual Technical Conference and Exhibition, Denver, CO, October 6-9.

Kraus, W.P., McCaffrey, W.J., and Boyd, G.W.: "Pseudo-Bubble Point Model for Foamy Oil," paper CIM 93-45 presented at the 1993 CIM Annual Technical Meeting, Calgary, AB, May 9-12.

Lolley, C.S. and Richardson, W.C.: "Compositional Input for Thermal Simulation of Heavy Oils with Application to the San Ardo Field," paper SPE 37538 presented at the 1997 SPE Thermal Operations and Heavy Oil Symposium, Bakersfield, CA, Feb. 10-12.

Loughead, D.J. and Saltuklaroglu, M.: "Lloydminster Heavy Oil Production - Why so Unusual?" paper presented at the 1992 Annual Meeting of the Canadian Heavy Oil Association, Calgary, March 11.

Maini, B.B., Sarma, H.K., and George, A.E.: "Significance of Foamy-Oil Behaviour in Primary Production of Heavy Oil," *JCPT* (1993) Nov. 50-54.

Metwally, M. and Solanki, S.C.: "Heavy Oil Reservoir Mechanisms, Lindberg and Frog Lake Fields, Alberta, Part I: Field Observations and Reservoir Simulation," paper CIM 95-63 presented at the 1995 CIM Annual Technical Meeting, Banff, AB, May 14-17.

Mirabal, M. de, Gordillo, R., Rojas, G., Rodriguez, H., and Huerta, M.: "Impact of Foamy Oil Mechanism on the Hamaca Oil Reserves, Orinoco Belt-Venezuela," paper SPE 36140 presented at the 1996 SPE Latin American and Caribbean Petroleum Engineering Conference, Trinidad, April 23-26.

Mirabal, M. de, Rodriguez, H., and Gordillo, R.: "Production Improvement Strategy for Foamy Hamaca Crude Oil: A Field Case," paper SPE 375554 presented at the 1997 SPE Thermal Operations and Heavy Oil Symposium, Bakersfield, CA, Feb. 10-12.

Shen C. and Batycky, J.: "Some Observations of Mobility Enhancement of Heavy Oil Flowing Through Sand Pack under Solution Gas Drive," paper CIM 96-26 presented at the 1996 CIM Annual Technical Meeting, Calgary, AB, June 10-12.

Sheng, J.J., Maini, B.B., Hayes, R.E., and Tortike, W.S.: "A Non-Equilibrium Model to Calculate Foamy Oil Properties," paper CIM 95-19 presented at the 1995 CIM Annual Technical Meeting, Banff, AB, May 14-17.

Smith, G.E.: "Fluid Flow and Sand Production in Heavy Oil Reservoirs under Solution Gas Drive," *SPEPE* (1988) May 169-177.

Table 1. Rock data

	Light oil run	Heavy oil run
Permeability, Darcy	16	16
Porosity, %	36	36
Diameter, cm	5.1	5.1
Height, cm	23.5	21.5
Pore Volume, cm ³	270	245
Volume of the window, cm ³	3.9	8.2

Table 2. Fluid data

	Light model oil	Heavy oil
Density at 75 F, g/cm ³	0.724	0.9854 ¹
Molecular Weight	142	455 - 468 ¹
Viscosity at 75 F, cp	0.9	56000 ¹
GOR, vol/vol	13	6
Bubble Point Pressure, psig	280	300

1. Data from Lolley and Richardson [1997]

Table 3. Data of the light and heavy oil experiments

	Light model oil, Run 1	Light oil, Run 2	Heavy oil Run 1
Initial rate of expansion, cm ³ /hr	0.018	0.018	0.041
Second rate of withdrawal, cm ³ /hr	0.054 (at 0.58 cm ³)	0.054 (at 0.58 cm ³)	0.082 (at 5.95 cm ³)
Third rate of withdrawal, cm ³ /hr	0.108 (at 3.22 cm ³)	0.108 (at 3.22 cm ³)	
Initial rate of pressure drop,	50	50	140

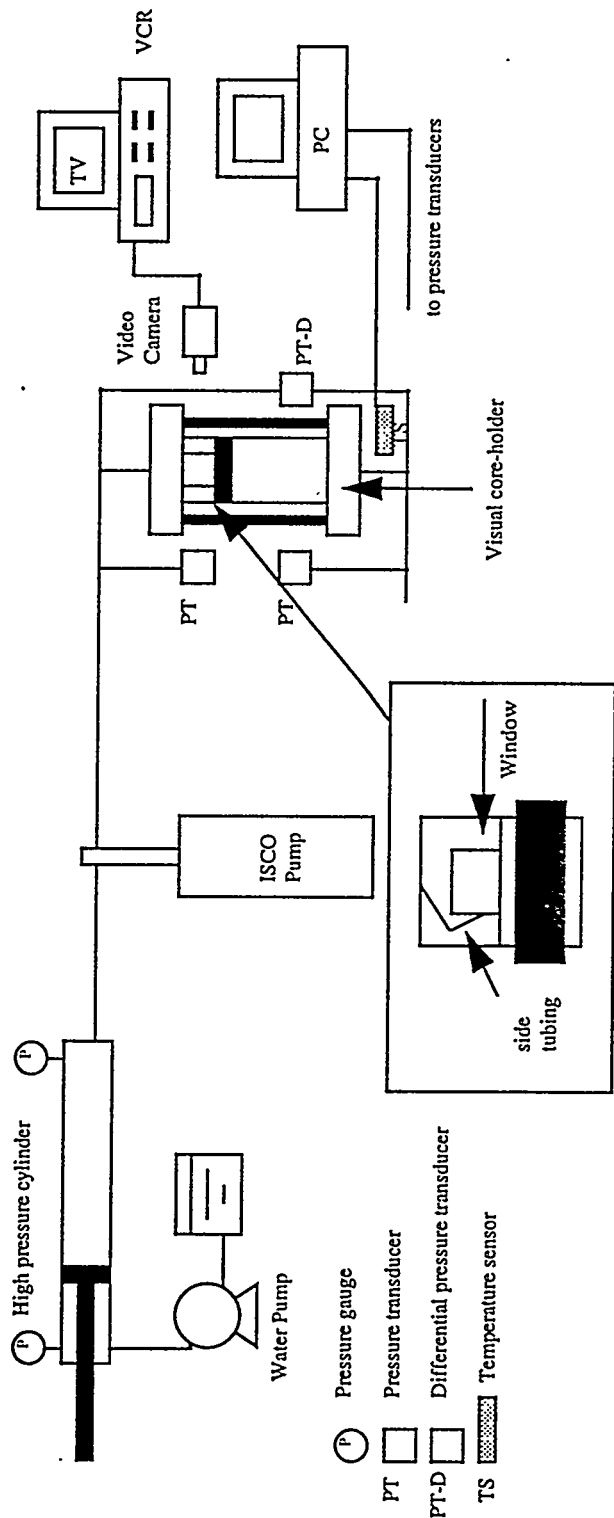


Figure 1. Schematic diagram of the setup

Figure 2. Volume change of the oleic phase vs. time

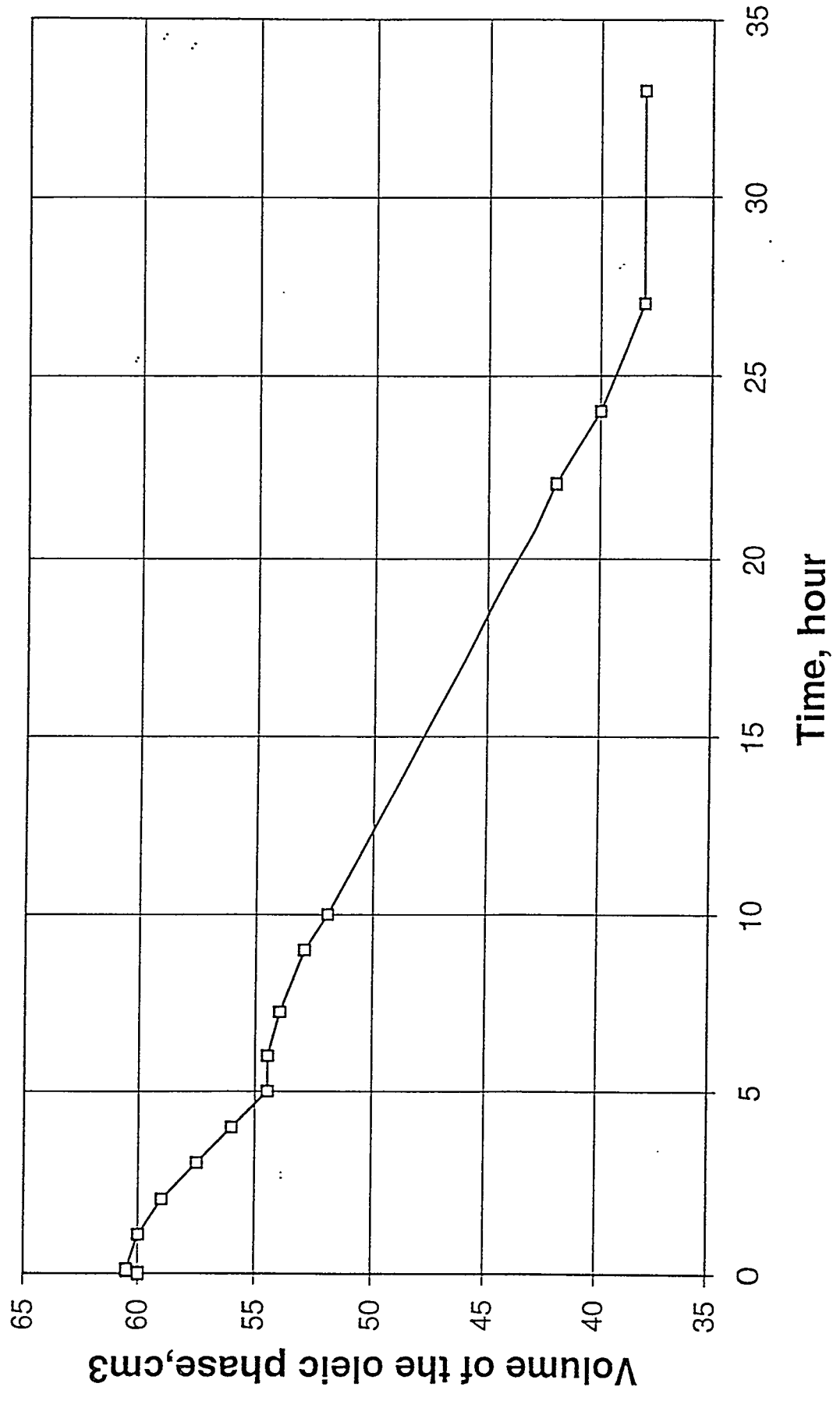


Figure 3. Pressure vs. volume expansion for Run 1 and Run 2

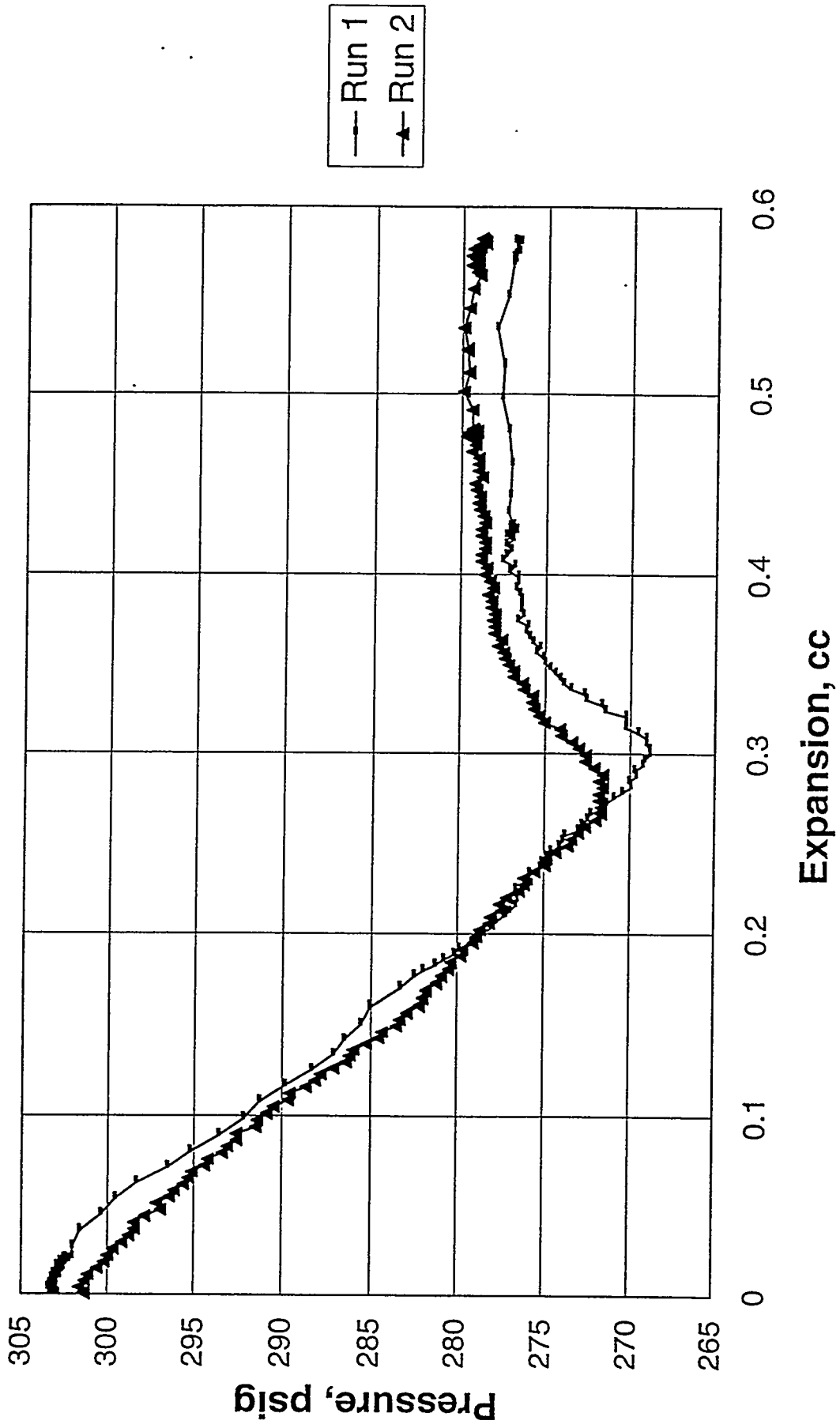
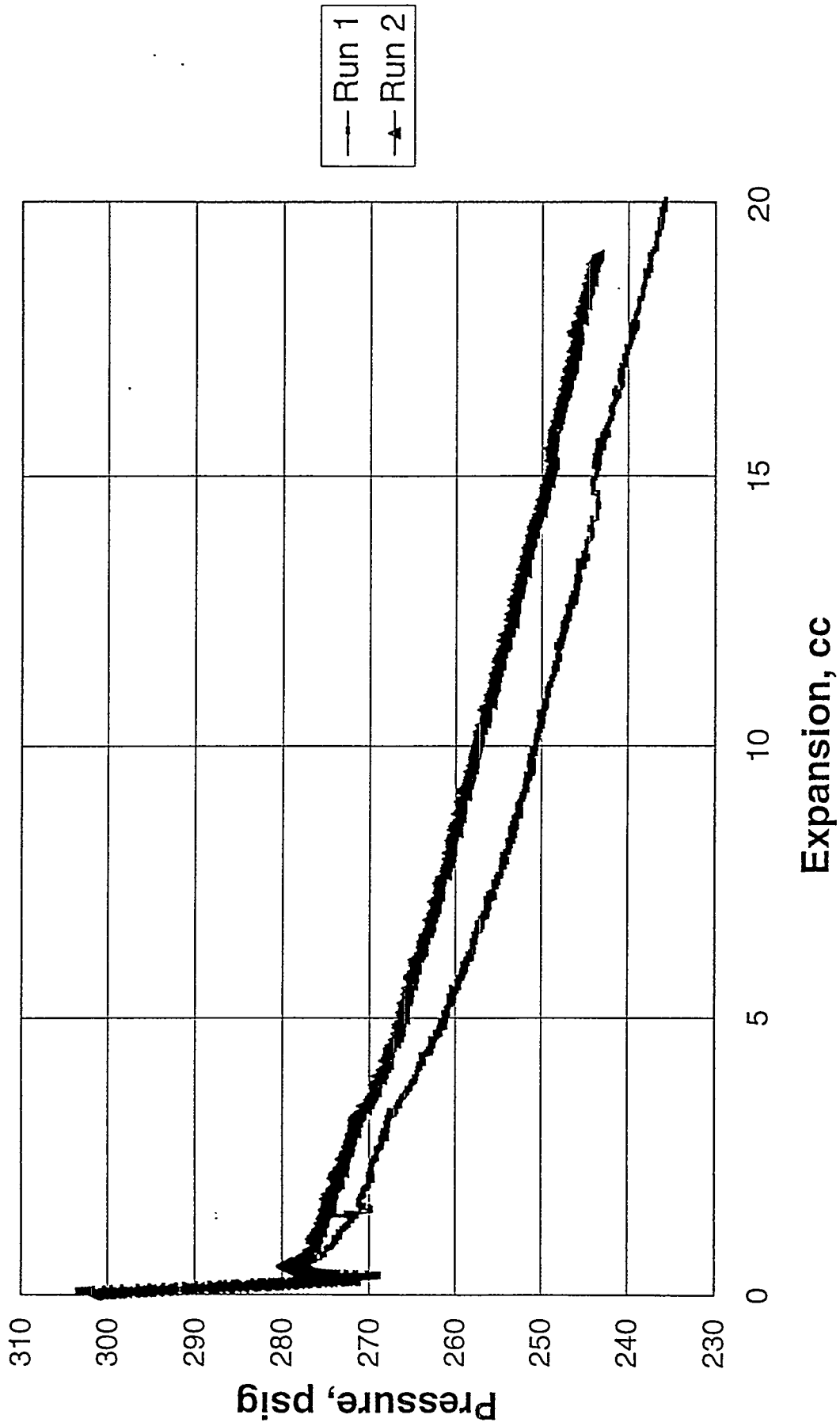


Figure 4. Pressure vs. volume expansion for Run 1 and Run 2



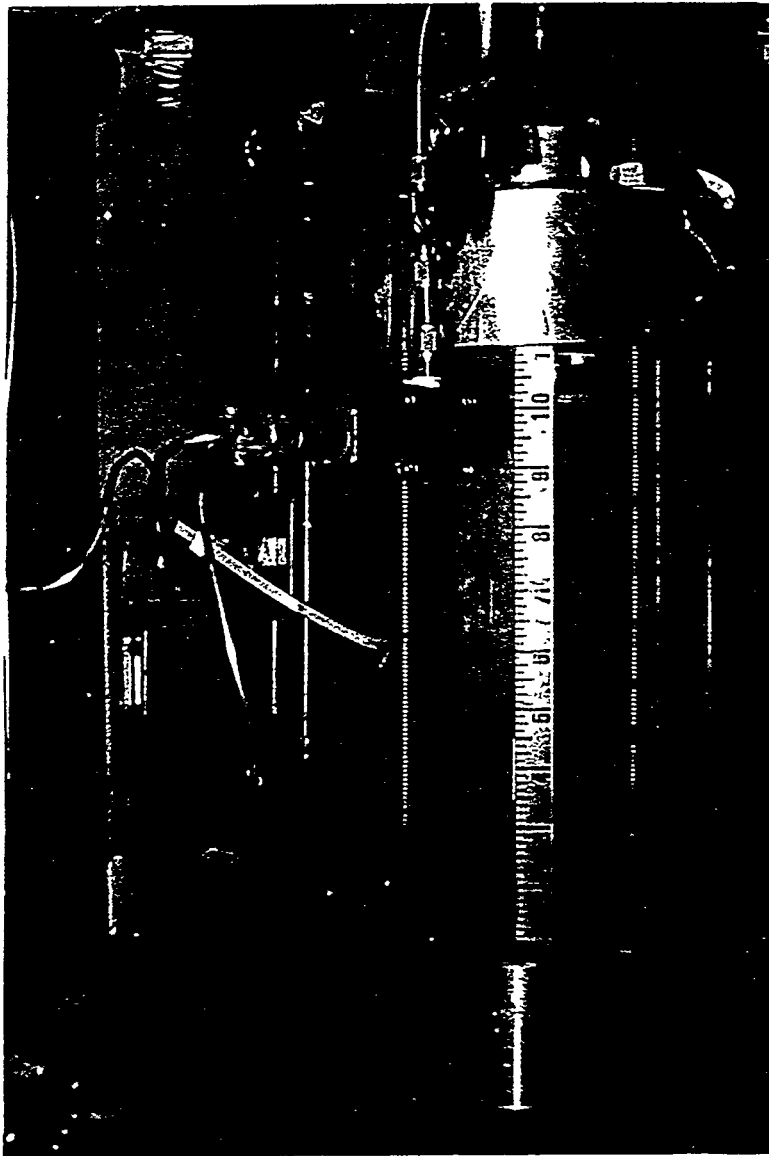


Figure 5. Gas pattern in Run #2, Expansion = 5.7 cm^3

Figure 6. Gas saturation in the sand pack for Run 1 and Run 2

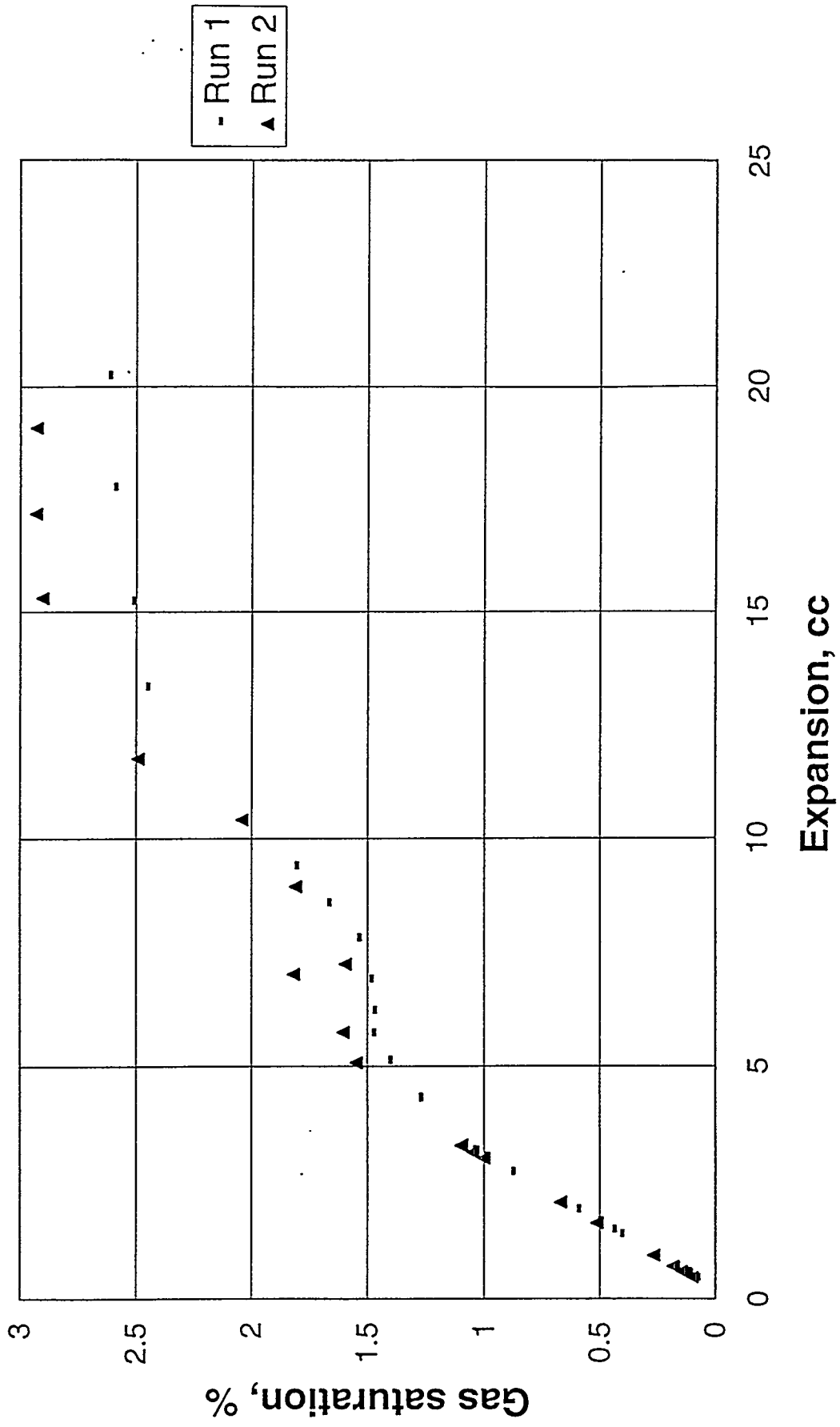


Figure 7. Pressure vs. volume expansion for the heavy oil run

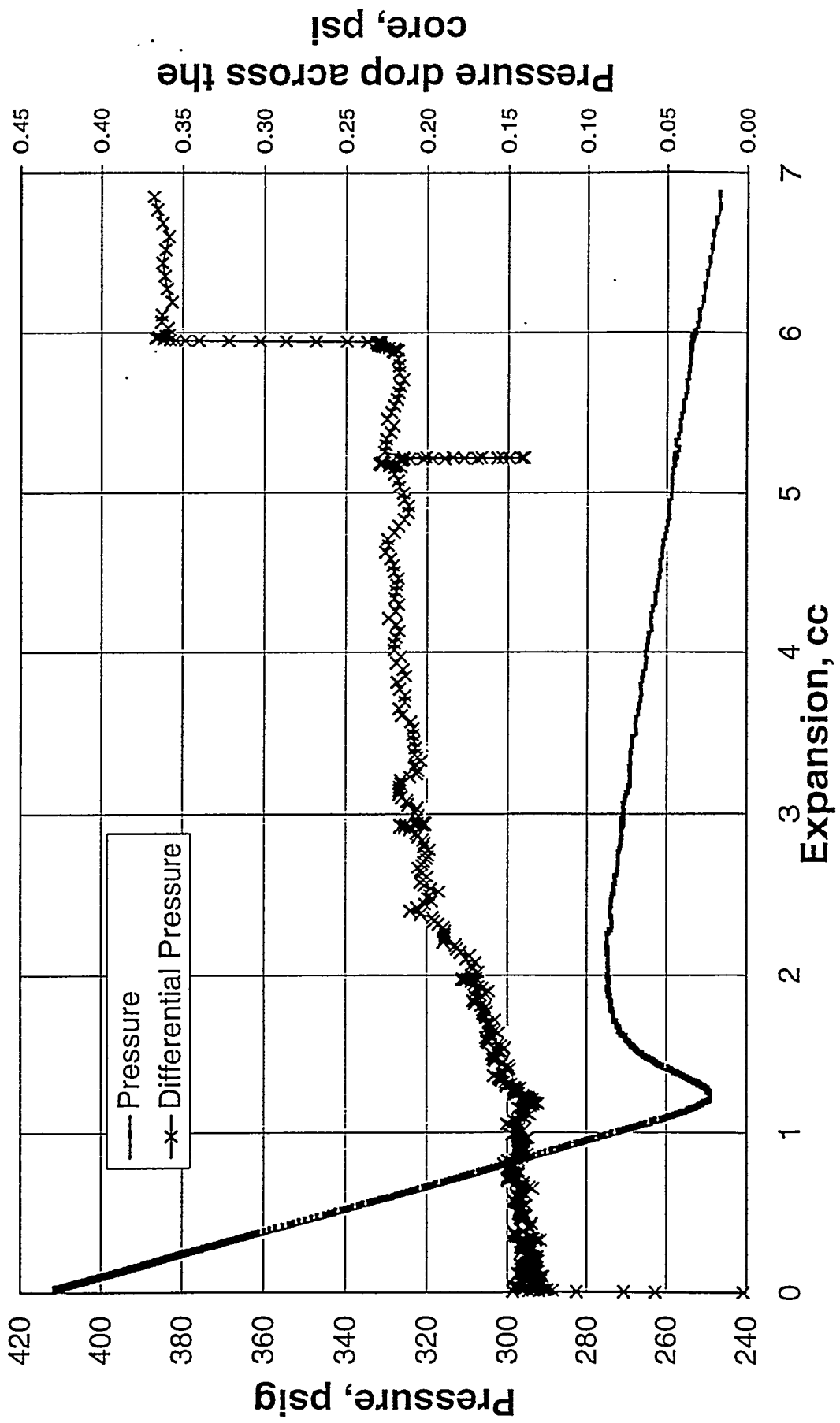


Figure 8. Pressure vs. volume expansion for the heavy oil run

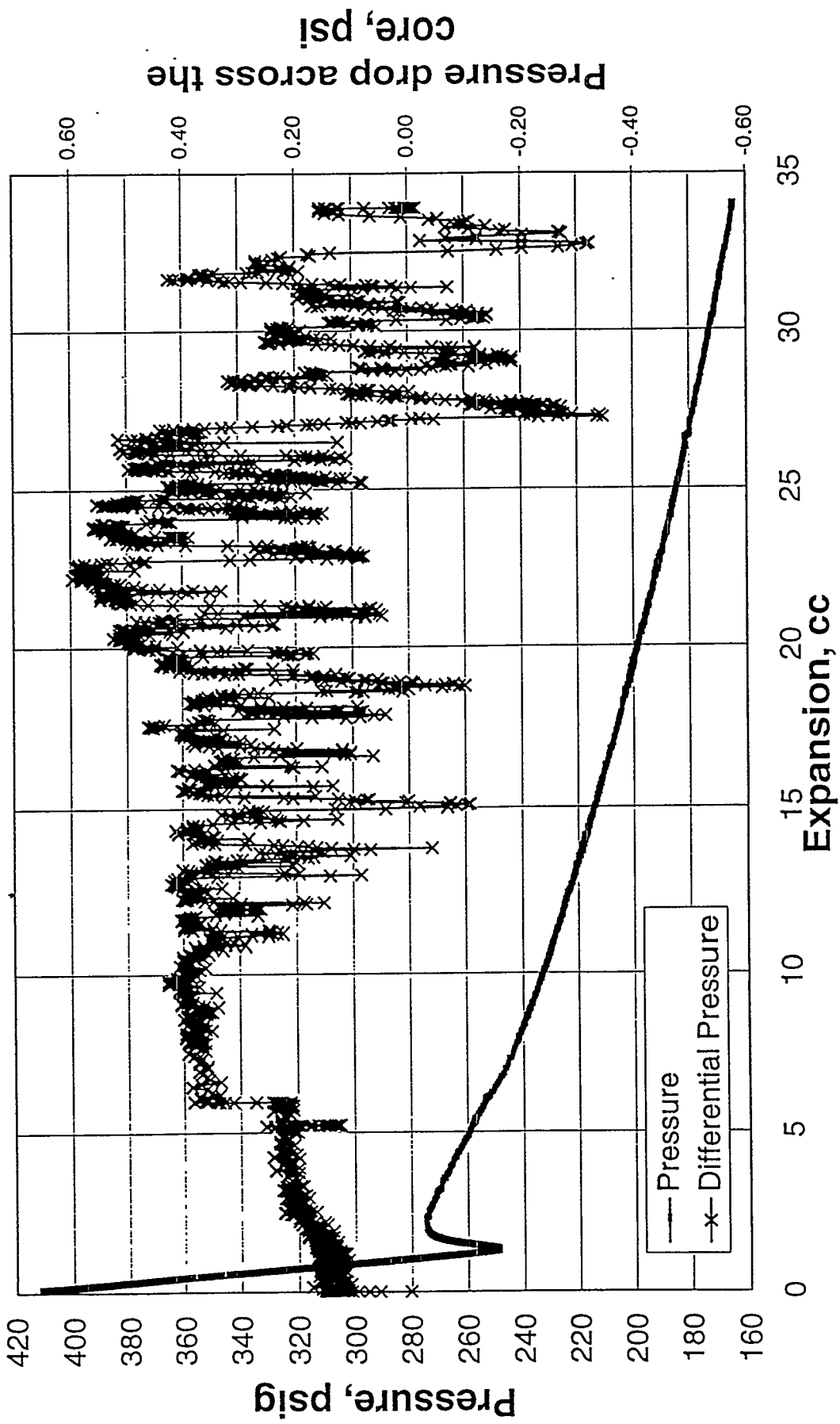


Figure 9. Gas saturation in the sand pack for the heavy oil run

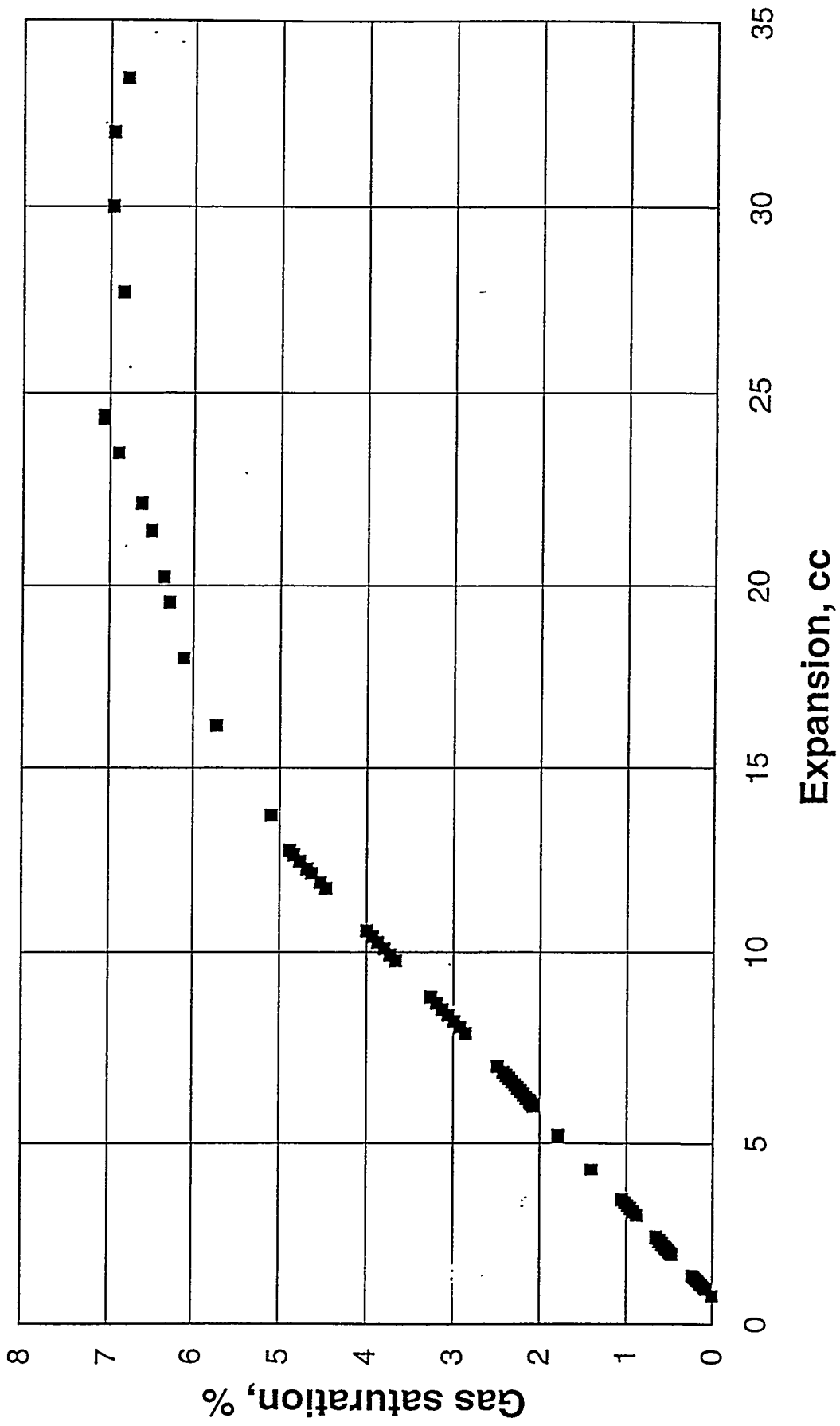
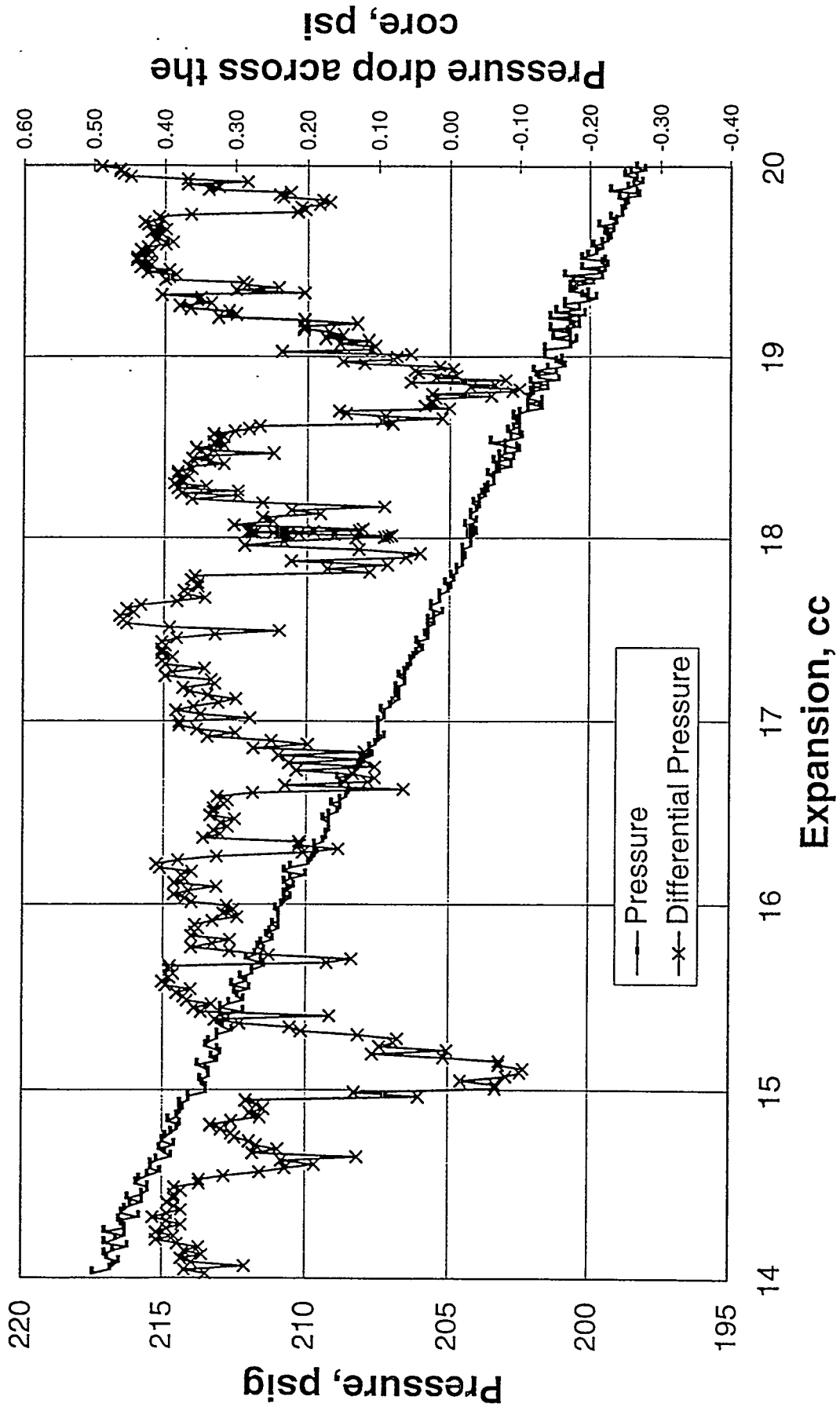


Figure 10. Pressure vs. volume expansion for the heavy oil run



**RESERVOIR ENGINEERING RESEARCH
INSTITUTE**

**PROJECT 6a: WATER INJECTION IN
FRACTURED/LAYERED MEDIA**

Water Injection in Water-Wet Fractured Media

4Q.96

October 1 through December 31, 1996

Abbas Firoozabadi
Mehran Pooladi-Darvish

Water Injection in Water-Wet Fractured Porous Media

Summary

We have carried out a number of experiments on 1) a single block, and 2) stacked blocks of the Kansas outcrop chalk. The results on the single matrix block conclusively establish that the immersion of a block in the wetting phase gives a pessimistic recovery compared to the case of gradual water-oil contact movement in the fractures surrounding the matrix-block.

Water injection in the stacked blocks reveal that water displacement in the Kansas outcrop chalk is very efficient - even more efficient than water displacement in the high permeability Berea.

Introduction

In a recent theoretical study¹ (Pooladi-Darvish and Firoozabadi, 1996), we have shown that water injection in water-wet fractured media can be very efficient due to co-current imbibition. In order to quantify the imbibition process, we have embarked on an experimental research effort to measure the water-displacement efficiency in tight matrix blocks from the Kansas outcrop chalk. The chalk permeability is in the 2-5 md range, with a porosity close to 30 percent. The Kansas outcrop chalk is very similar to the Ekofisk chalk in the North Sea.

We have done extensive measurements of water displacement efficiency in the Berea fractured media² (Pooladi-Darvish and Firoozabadi, 1996). It will be interesting to compare water displacement efficiency in the Berea and Kansas outcrop fractured media.

Kansas outcrop chalk is strongly water-wet. Therefore, the first phase of this study includes water injection in a strongly water-wet fractured media. In the second step, we plan to alter the chalk wettability to a more oil-wet and a mixed-wet state and then study water displacement efficiency.

In the following, we will present the results for 1) a single block, and 2) a stack of 12-matrix blocks.

Apparatus

The apparatus including the coreholder are similar to what has been described in Ref. 2. Only the core materials are different. Normal decane was used as the oleic phase and 1% NaCl solution as the aqueous phase. Apparatus schematic is shown in Fig. 1.

Experimental Results

Single Block

A single block of the Kansas outcrop chalk (see Fig. 2), with dimensions $A = 6.35$ cm, $B = 18.75$ cm, and $C = 30.48$ cm was housed in the visual coreholder. The block is surrounded by top, bottom, and four side fractures. The fracture PV is estimated to be 26 cm^3 , and the matrix PV = 1050 cm^3 . The effective permeability of the combined fracture-matrix is calculated by downward single phase flow of nC_{10} ; $k_e = 16$ darcy.

Three different tests were performed by injecting water from the bottom. The results are presented next.

Test 1 - (Injection rate = $22.1 \text{ cm}^3/\text{hr.}$): In the first test on the single chalk block, water was injected at a low rate of $22.1 \text{ cm}^3/\text{hr.}$ Fig. 3 shows the plot of nC_{10} recovery vs. PV water injection. Before breakthrough, nC_{10} production and water injection rates are the same. Oil recovery at breakthrough is 62 percent. Very little oil was produced after water breakthrough. The residual oil saturation to water is therefore, $S_{or} = 38\%$.

Fig. 4 depicts the water-oil level in the vertical fractures (FWL) surrounding the matrix. (The FWL in all four fractures are shown by the same symbol for all the tests). As the figure shows, the FWL moves faster initially in two of the fractures. For $PV > 0.15$, the FWL in all four fractures advances with the same speed to $PV = 0.4$; thereafter water advances faster in one of the fractures. FWL reaches the block top at $PV \approx 0.6$ and afterwards only water is produced.

During the experiment, for the most part, water was observed to be moving in the matrix about 0.5 cm ahead of the FWL. In the course of the experiment, we did not observe any oil production below the FWL which implies the process is co-current imbibition.

Test 2 - (Injection Rate = $140 \text{ cm}^3/\text{hr.}$): In the second test, the rate of injection was increased to $140 \text{ cm}^3/\text{hr.}$ Fig. 3 depicts the recovery data; breakthrough occurred at $PV = 0.39$. Oil production rate decreased continuously after breakthrough; at $PV = 1$, the recovery was close to 60 percent. The FWL data are shown in Fig. 4. This figure shows that to $PV = 0.03$, FWL moves fast. Beyond $PV = 0.03$, FWL in all four side fractures moves slowly. Toward the end beyond 0.3 PV injection, FWL velocity increases..

In this test, while the FWL was moving in the fractures, very small droplets of oil were visible forming on the matrix surface, and then flowing towards the FWL.

Test 3 - (Injection Rate = $276 \text{ cm}^3/\text{hr.}$): The rate for test 3 was set twice the rate in test 2. Fig. 3 shows the recovery data. The breakthrough occurred at $PV = 0.20$. Oil production rate decreased continuously after breakthrough. The ultimate recover is 61 percent -- very similar to the previous two tests. Recovery at $PV = 1$ injection is over 50%.

Fig. 4 shows the FWL vs. PV injection. Initially the FWL moves very fast; the level moves to 15 cm height at 0.04 PV injection. The FWL then moves at a lower speed. In this high injection rate test as soon as water filled the fracture space, very small droplets of oil were visible, forming on the rock surface. We also observed oil production in the form of small droplets underneath the block flowing to the FWL.

In addition to the above three tests, a fourth test was performed on the single block by immersing it in water and measuring the rate of oil production.

Test 4 - (Immersed Block) : In this test the block was immersed in water. The fractures surrounding the block and the top fracture are very large (thickness ≈ 1 cm). Fig. 5 shows the recovery vs. time for test 4 and the two previous tests. Note that the production for this test is very inefficient compared to the previous tests. Recovery for test 4 is by counter-imbibition which is much slower than all other tests. The final recovery is close to tests 2 and 3.

Next we present the results on the 12- block stack.

12-Block Stack

We conducted two tests on a stack of 12-matrix blocks (see Fig. 2). The PV of the total matrix-fracture system is 13900 cm^3 . The PV of the fracture network is estimated to be $700 \text{ cm}^3/\text{hr}$. The matrix porosity is 29.6 percent. The effective permeability of the fracture-matrix system is estimated to be in the 13-21 darcy by measuring single phase flow across the system in the vertical direction. The effective permeability was 13 darcy for test 5 and 21 darcy for test 6 which are described in the following.

Test 5 - (Injection Rate = $151 \text{ cm}^3/\text{hr}$): Fig. 6 shows the recovery plot for test 5; the breakthrough recovery is 66 percent (the PV in Fig. 6 is the total matrix and fracture PV). Very little oil was produced after breakthrough.

Fig. 7 graphs the FWL; it took an hour to observe the water in the side fractures. The delay in water appearance could be partly due to the imbibition in the bottom part of the system. At $t \approx 1$ hr, we noticed that the location of water front in the matrix was about 0.5 cm above FWL. Later on, the water front in the matrix was about 0.5 to 2.5 cm ahead of the FWL. This observation can be interpreted that the oil production is entirely from the matrix above the FWL as a result of co-current imbibition. As Fig. 7 indicates, the FWL is very uniform in all side vertical fractures. This figure also shows that water reaches the top of the first-, second-, third-, and fourth-row blocks at PV = 0.15, 0.32, 0.46, and 0.66, respectively. Oil droplets did not form below the FWL. All indications are that the contribution of the counter-current imbibition for this test is negligible.

Test 6 - (Injection Rate = $445 \text{ cm}^3/\text{hr}$): The rate for this test was selected on the basis of test 2, and it was expected that the results for test 2 and 6 are comparable.

Fig. 6 shows the recovery; oil recovery at breakthrough is 64 percent. Only 150 cm³ of oil was produced after the breakthrough to PV injection of 1.

Fig. 7 shows the FWL vs. injection PV; water appeared in the side fractures at $t \approx 7$ min. Similar to the previous test, the FWL in all four vertical fractures were very close to each other. Water reached the top of the first-, second-, third-, and fourth-row matrix blocks at 0.12, 0.3, 0.41, and 0.64 PV injection, respectively.

In this test, we observed some oil flow in the form of droplets patched between the rock surface and the glass wall. Small spherical droplets of oil were also observed while the FWL was rising along the third-row blocks from the bottom in one of the side fractures. In this fracture, the aperture is estimated to be larger than the rest. However, the contribution of counter-current imbibition to the total production is very small. Oil production after breakthrough was less than 2% of the total recovery. The results from this test indicate higher displacement efficiency than test 2.

Comparison to the Berea Blocks

Fig. 8 shows the recovery data for the 12-matrix block of the high permeability Berea² ($k=650$ md). Surprisingly, water injection in the Berea stack is less efficient than the tight outcrop chalk. Breakthrough occurs earlier and the ultimate recovery is also less.

Conclusions and Future Plan

It has now been experimentally established that the co-current imbibition process is more efficient than the counter-current imbibition based on the results from tests 1 to 4. However, to quantify the imbibition process, we need to develop a model to analyze the results of various experiments by an appropriate numerical model. We intend to carry out one more test for the 12-block system at a higher rate, and have a duplicate for test 4. Then the emphasis will be on the analysis of the experiments.

The experiments have also established the high efficiency of water injection in the Kansas outcrop chalk and its state of complete water-wetness.

References

1. Pooladi-Darvish, M., and Firoozabadi, A.: "Co-Current and Counter-Current Imbibition in Water-Wet Matrix Blocks," RERI 1Q.96, May 1996.
2. Pooladi-Darvish, M., and Firoozabadi, A.: "Water Injection in Fractured Media," RERI 3 Q.96, Oct. 1996.

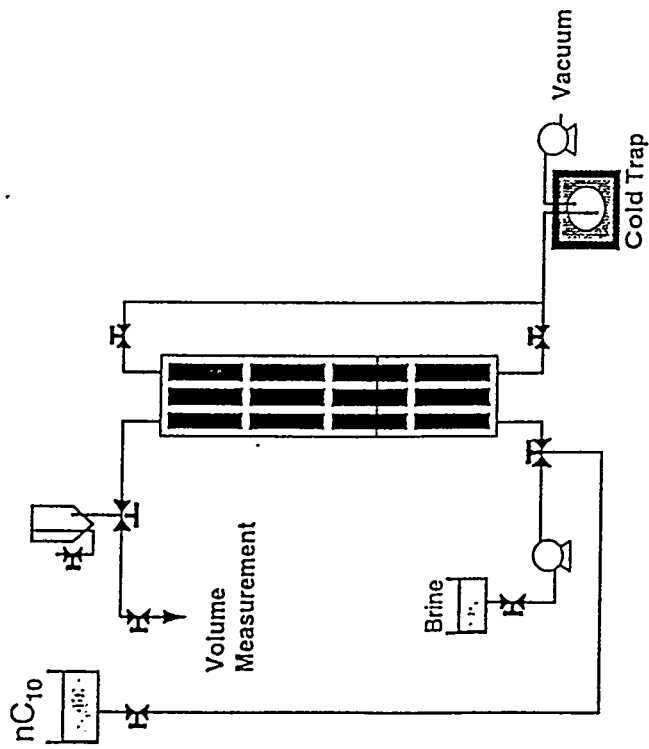


Figure 1. Schematic diagram of the apparatus.

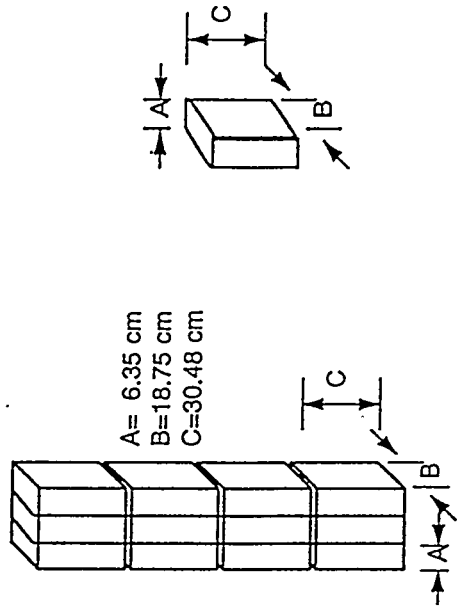


Figure 2. The rock assembly for Tests 1, 2, 3 and 4 (right hand diagram) and for Tests 5 and 6 (left hand diagram).

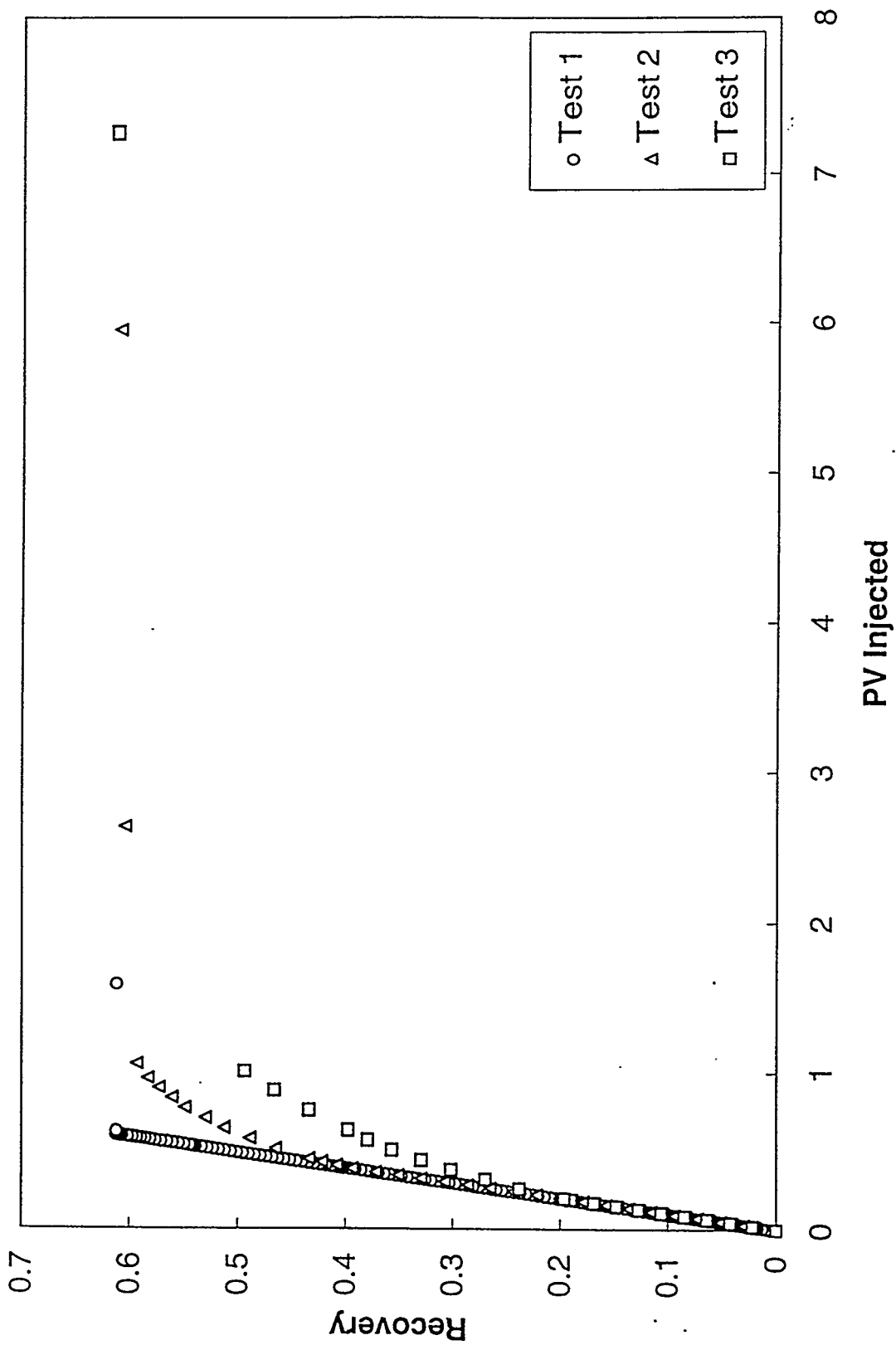


Fig.3-Recovery performance of tests 1, 2, and 3.

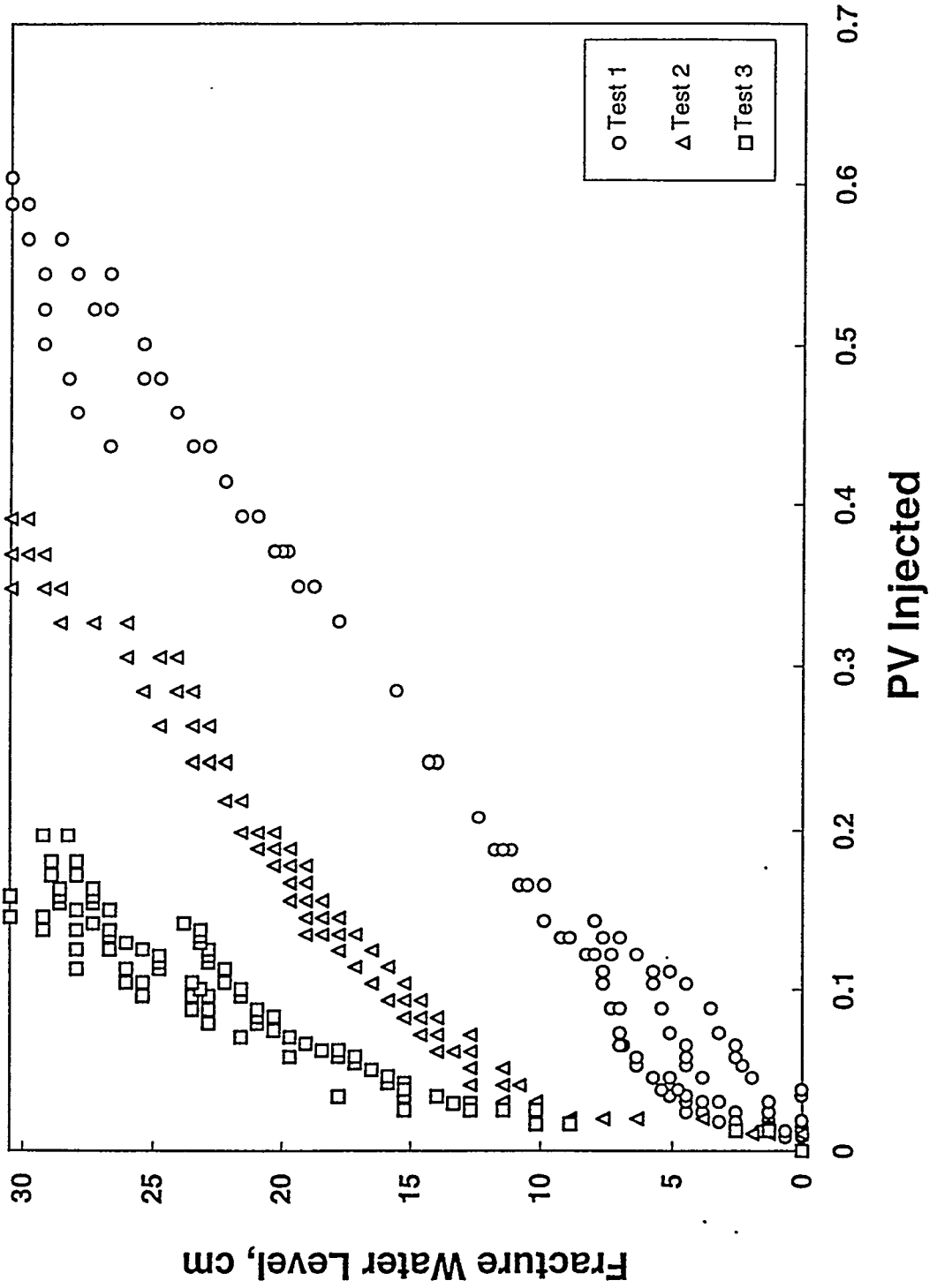


Fig.4-Fracture water level for tests 1, 2, and 3

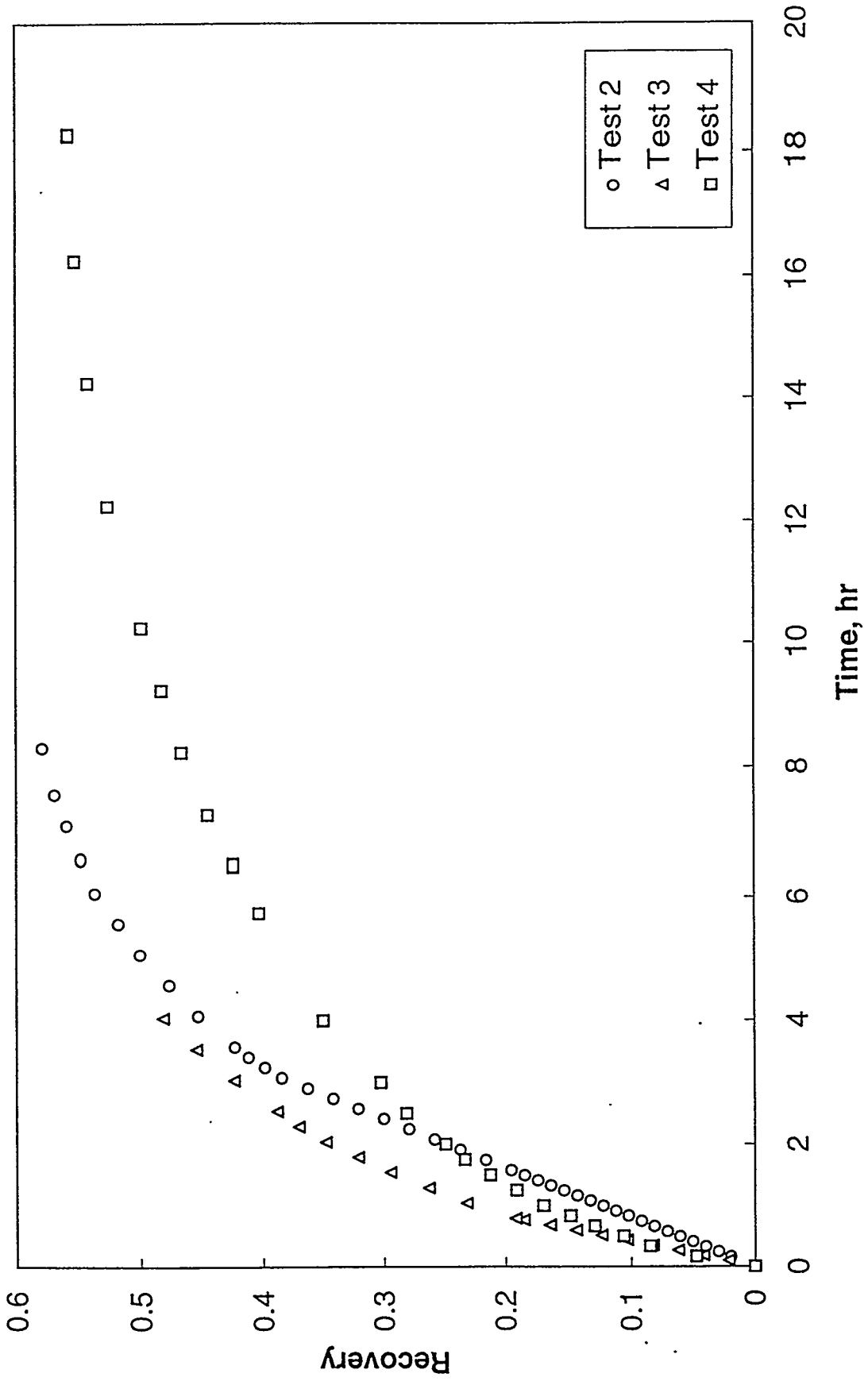


Fig.5-Recovery performance of tests 2, 3 and 4.

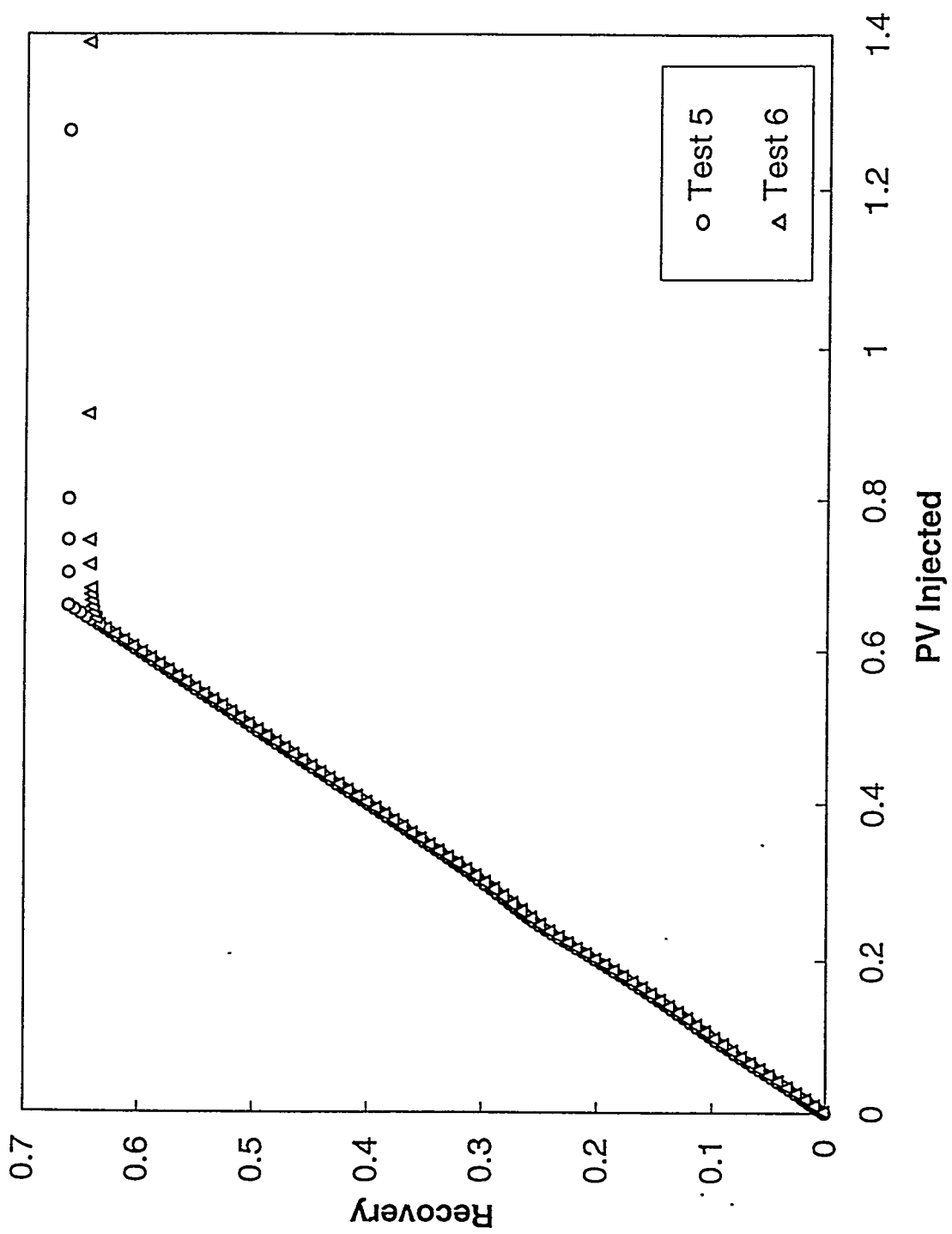


Fig. 6-Recovery performance of tests 5 and 6.

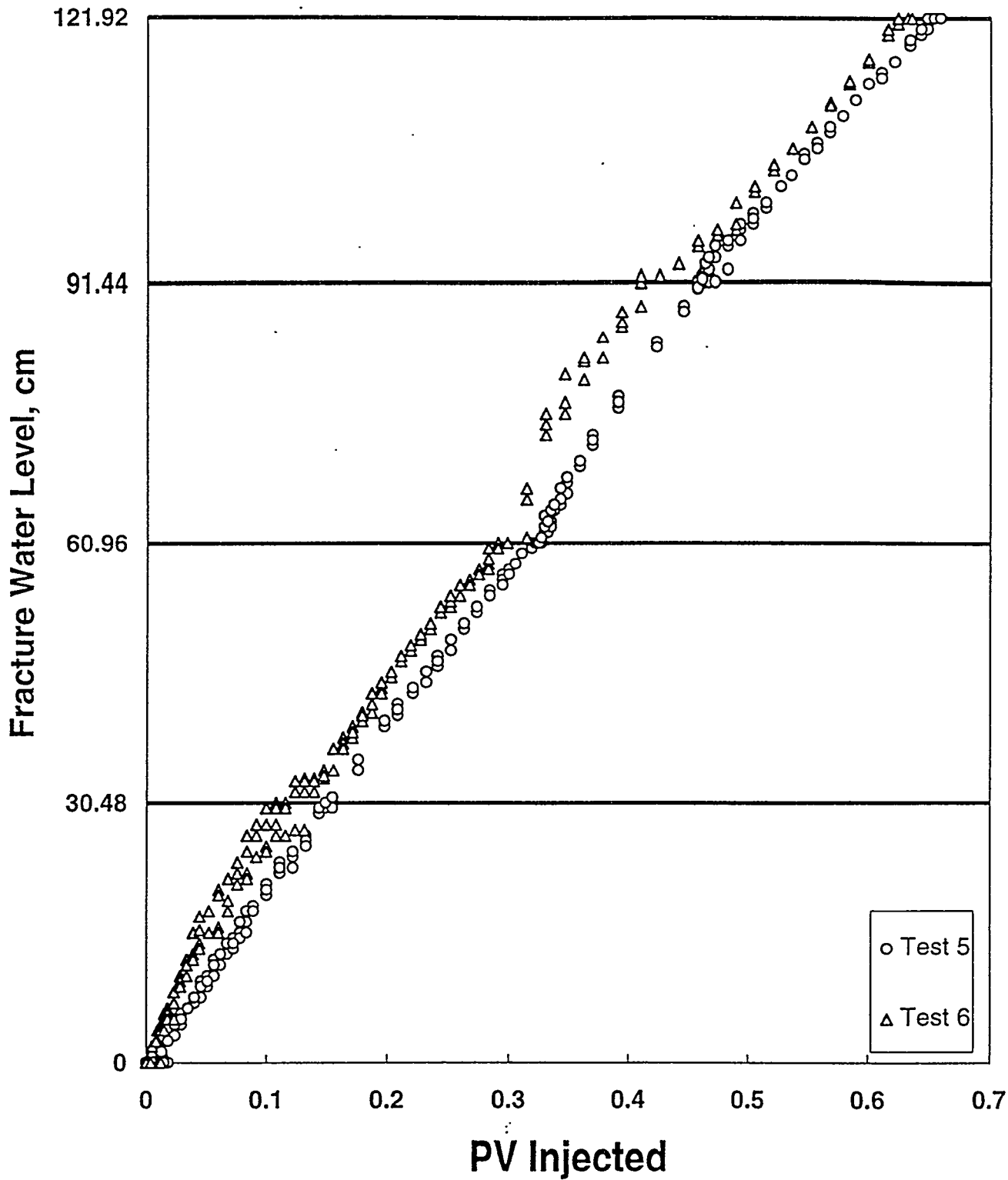


Fig. 7 - Fracture water level for tests 5 and 6.

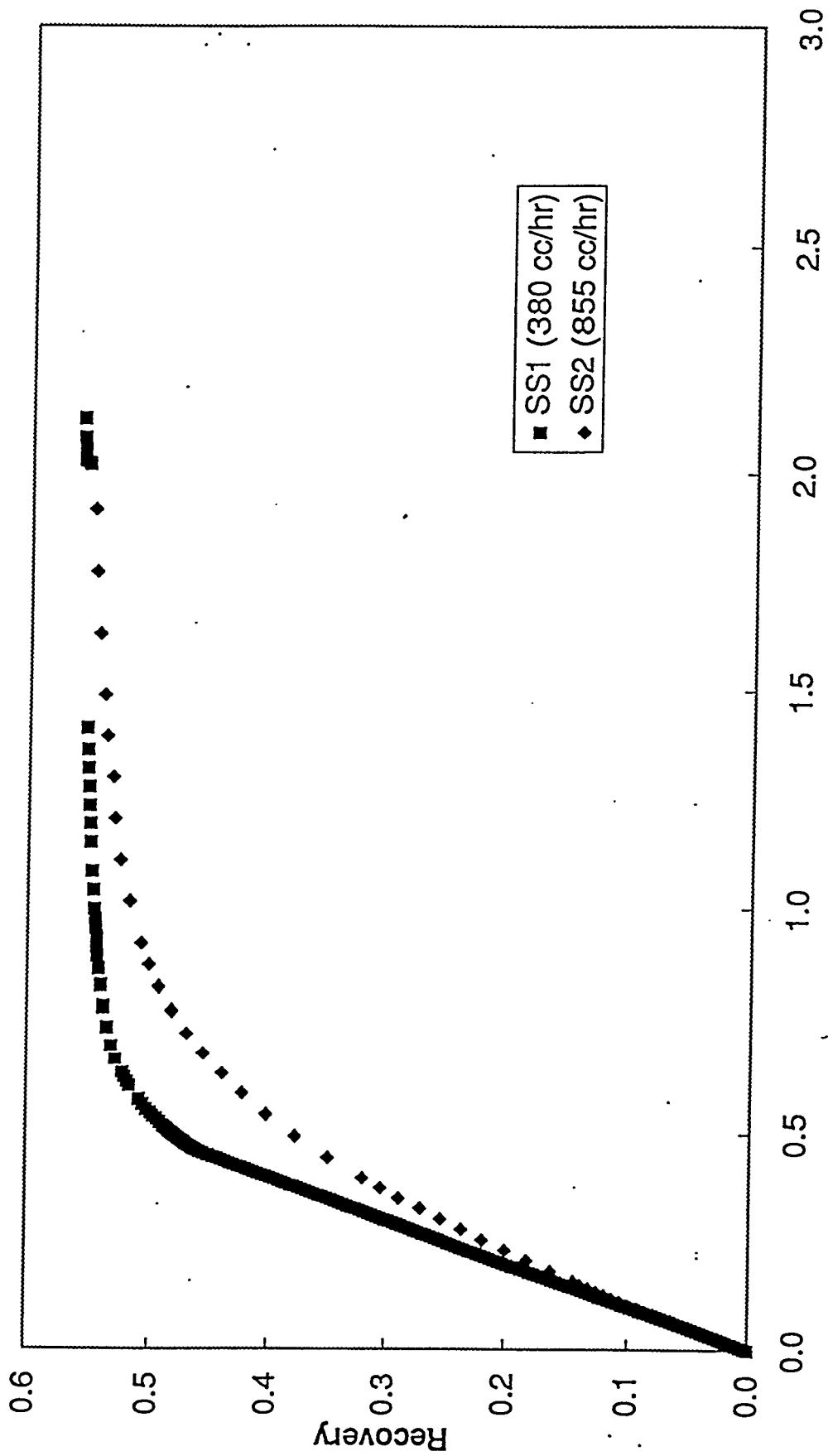


Figure 8. Recovery performance of the 12-block Berea stack.